Engineering of Hollow Periodic Mesoporous Organosilica Nanorods for Augmented Hydrogen Clathrate Formation

Geert Watson [a, 1], Nithin B. Kummamuru [b, 1], Sammy W. Verbruggen [b, c], Patrice Perreault [d, e], Maarten Houlleberghs [f], Eric Breynaert [f], Johan Martens [f], Pascal Van Der Voort [a, *]

[a] Centre for Ordered Materials, Organometallics and Catalysis (COMOC), Department of Chemistry, Ghent University, Krijgslaan 281-S3, 9000 Ghent, Belgium.

[b] Sustainable Energy Air & Water Technology (DuEL), Department of Bioscience Engineering, University of Antwerp, Groenenborgerlaan 171, 2020 Antwerpen, Belgium.

[c] NANOlab Center of Excellence, University of Antwerp, Groenenborgerlaan 171, 2020 Antwerpen, Belgium.

[d] Faculty of Science, Instituut voor Milieu & Duurzame Ontwikkeling (IMDO), Campus Groenenborger – Building V.612, Groenenborgerlaan 171, 2020 Antwerpen, Belgium.

[e] University of Antwerp, BlueApp, Olieweg 97, 2020 Antwerpen, Belgium.

[f] Centre for Surface Chemistry and Catalysis, NMRCoRe - NMR - XRAY - EM Platform for Convergence Research, Department of Microbial and Molecular Systems (M2S), KU Leuven, Celestijnenlaan 200F, 3001, Leuven, Belgium.

* Corresponding author. E-mail address: pascal.vandervoort@ugent.be

[1] Contributed equally to this work.

ABSTRACT

Hydrogen (H_2) storage, in the form of clathrate hydrates, has emerged as an attractive alternative to classical storage methods like compression or liquefaction. Nevertheless, the sluggish enclathration kinetics along with low gas storage capacities in bulk systems is currently impeding the progress of this technology. To this end, unstirred systems coupled with porous materials have been shown to tackle the aforementioned drawbacks. In line with this approach, the present study explores the use of hydrophobic periodic organosilica nanoparticles, later denoted as Hollow Ring-PMO (HRPMO), for H_2 storage as clathrate hydrates at mild operating conditions (5.56 mol% THF, 7 MPa, and 265-273 K). The surface of the HRPMO nanoparticles was carefully decorated/functionalized with THF-like moieties, which are well-known promoter agents in clathrate formation when applied in classical, homogeneous systems. The study showed that, while the non-functionalized HRPMO can facilitate the formation of binary H_2-THF clathrates, the incorporation of surface-bound promotor structures enhances this process. More intriguingly, tuning the concentration of these surface-bound promotor agents on the HRPMO led to a notable effect on solid-state H_2 storage capacities. An increase of 3% in H_2 storage capacity, equivalent to 0.26 wt.%, along with a substantial increase of up to 28% in clathrate growth kinetics, was observed when an optimal loading of 0.14 mmol/g of promoter agent was integrated into the HRPMO framework. Overall, the findings from this study highlight that such tuning effects in solid-state have the potential to significantly boost hydrate formation/growth kinetics and H_2 storage capacities, thereby opening new avenues for the ongoing development of H_2 clathrates in industrial applications.

KEYWORDS: Hydrogen storage, Hydrogen clathrates, Hydrophobic porous solids, Promotors, Tetrahydrofuran (THF), Solid state tuning.

1. Introduction

While global energy demands are ever-increasing, the extraction and transport of fossil fuels have become progressively more taxing on the environment. On top of this, these resources are finite, so it is of vital importance that a transition to cleaner and more sustainable energy sources is made. Hydrogen (H_2), which is clean, carbon neutral, if produced from renewable resources, and has about 2.5 times more calorific value than fossil fuels is increasingly being seen as a crucial pillar of energy security for the associated governments/nations[1, 2]. This is evidenced by H_2 demand climbing 4% in 2022 from pre-pandemic levels of 91 million tonnes in 2019 to an estimated 180 million tonnes by 2030[3]. Given the significant use of H_2 now and in the coming decades, safety and suitability in storage and transportation are essential, however, these are the main limitations impeding the transition of innovative H_2 technologies from production to mobility or energy applications.

H_2, by virtue of its low density (0.08 g/l) requires a large volume for a given amount of energy and the classical H_2 storage approach in its molecular form includes compression, liquefaction, and cryo-compressed technologies[4]. Although these are the more established and mature technologies, they have a variety of drawbacks, such as expensive vessel costs to maintain high pressures (20-70 MPa), heaviness and bulkiness of gas cylinders, higher safety standards, high liquefaction energies, and boil-off losses up to 4% a day[5-8]. Other storage solutions, such as Adsorption[9-15], Metal hydrides[16-22], Liquid Organic Hydrogen Carriers (LOHC)[23], Ammonia[24], etc., have been proposed in addition to these conventional methods, and tremendous research on these materials is actively being developed in pursuit of

68 better H_2 storage capacities to confront their sluggish kinetics, poor reversibility, cycling
69 instability, and thermal management issues[1, 25-28].

70 Aside from the above-mentioned H_2 storage systems, hydrate/clathrate based (trapping H_2 in
71 hydrate cages) technology is relatively new and promising, attracting significant interest owing
72 to its advantages. Essentially, trapping H_2 in hydrate cages is environmentally favorable as
73 water (H_2O) is the principal storage medium, with extremely low concentrations of the
74 promoter molecules (< 6 mol%) if incorporated[29-31]. Second, the stored molecular H_2 can
75 be quickly recovered by pressure or temperature swings with no loss of H_2O or promoter
76 molecules. Gas hydrates or Clathrates hydrates, are ice-like crystalline materials formed under
77 favorable thermodynamic conditions when suitable guest (usually apolar) molecules are
78 trapped/encaged within the 3-dimensional H_2 bonded host (H_2O) molecules[32]. Pure H_2 forms
79 a classical sII hydrate structure with 136 H_2O molecules having a skeleton of sixteen
80 dodecahedron (small) and eight hexakaidecahedron (large) cages between 0.75 and 3.1 GPa at
81 295 K[33]. Although multiple H_2 occupancy in small and large cages enhances storage
82 capacity, the pressures mentioned above render them undesirable for any commercial or
83 industrial applications[30, 34-36]. In order to make it industrially viable, incorporating a
84 promoter molecule (tetrahydrofuran: THF) within the large cages, resulting in a binary H_2-THF
85 hydrate, demonstrated a substantial advancement in H_2 storage via hydrates at pressures as low
86 as 5 MPa and 279.6 K[31]. Despite a tremendous reduction in pressure conditions, the addition
87 of promoter molecules results in a low overall H_2 storage capacity as they occupy large cages
88 and leave only small ones for H_2. Nevertheless, Lee et al.[37] and other researchers[38]
89 reported to overcome this barrier by tuning the THF concentration from the stoichiometric
90 value of 5.56 mol% to a significantly lower value of 0.15 mol%, allowing H_2 to penetrate some
91 of the large cages. Conversely, many other researchers argue that the H_2 storage is independent

of the THF concentration and was unable to replicate equivalent storage capacities by tuning [39-42].

These groundbreaking and contentious findings paved the way for various strategies to improve H_2 storage via hydrate technology at moderate pressures and temperatures. Although significant studies have gained insights into the cage occupancies, overall storage capacities, and thermodynamics with various promoters (THF being reported as the best promoter thus far)[43-45], the authors believe that the constraints on mass transfer rate and enclathration kinetics have largely been overlooked, which is a significant impediment to foster this technology. The formation of hydrates from the bulk aqueous phase, in particular, is associated with a slow H_2 uptake rate due to insufficient contact/interaction between H_2 and H_2O or H_2O + promoter molecules, which can take up to a few hours or week to reach its maximal storage capacity[37, 40, 46, 47] and mechanical mixing which has the potential to accelerate the kinetics, has major limitations including high energy costs for stirring[48-50]. Other studies attempted to improve the mass diffusion by exposing the high pressure H_2 gas to pre-synthesized fine (< 45μm and 250 μm) THF-hydrate, however, this method is not compatible with continuous cycles as fine THF or other promoter hydrate particles relapse to bulk/liquid phase upon melting[40, 46, 51-53]. Given the challenges of synthesizing a binary H_2-THF hydrate from a bulk aqueous phase, it is imperative to emphasize on quiescent or unstirred systems that would provide accelerated kinetics in developing an efficient and cost-effective H_2 based technology. So far it is evident from the literature that decreasing the particle size or increasing the surface-to-volume ratio enhances the hydrate growth kinetics; however, there has been limited research available on boosting the kinetics of binary H_2-THF hydrates in an unstirred system packed with porous support materials[39, 51, 54-58]. It is important to note that when exploiting porous materials, multiple variables might contribute significantly to hydrate formation and kinetics such as pore volume, size, and network for gas saturation at the

interface, surface chemistry, and wettability. Contemporary work has shown that hydrophobic porous materials are more efficient than hydrophilic porous materials as H_2O molecules thermodynamically prefer to minimize their free energy by clustering near the hydrophobic surfaces which amplifies their mobility to promote hydrate nucleation and growth[57-68].

Considering the superiority of hydrophobicity, the present study attempts to design and develop such a porous material paving the pathway for faster enclathration kinetics of binary H_2 hydrates. Unlike activated carbons, having low dimensional pore networks, this study focuses on periodic mesoporous organosilicas (PMOs) that are carefully architectured in terms of pore sizes, network and are additionally functionalized with a highly mobile promoter molecule, THF (thanks to its extended ether chain linking the surface) to investigate their affinity towards forming H_2 hydrate with and without their use in the aqueous phase. Accordingly, the kinetics of binary H_2-THF hydrate formation and H_2 gas uptake are evaluated by exploiting the porous materials at 265 K, 269 K, and 273 K with an initial pressure of 7 MPa.

2. Experimental methods

2.1 Materials synthesis

Cetylammoniumbromide (CTAB), NH_3(aq) (25%), ethanol (EtOH), HCl_{aq} (37%), and tetraethyl orthosilicate (TEOS) were purchased from ChemLab. Pluronic F-127 was purchased from Merck Life Science. The organosilanes 1,1,3,3,5,5–hexaethoxy-1,3,5-trisilacyclohexane (HETSCH) and tetrahydrofurfuryloxypropyltriethoxysilane (THFPTES) were purchased from Gelest. All chemicals were used without any additional purification.

Hollow ring PMO (HRPMO) materials with a variation of the added amount of THF-like functionalities were prepared as candidates for the H_2-THF clathrate formation. Their synthesis is based on our earlier reported work[69]. In a typical synthesis, a closed flask of 500 ml was

charged with 290 ml (16 mol) H2O, 3 g (8.23 mmol) CTAB, 1.23 g (9.76 µmol) F-127 and 10 ml (0.134 mmol) NH3 (aq, 25%). The whole was left to stir at room temperature until a homogeneous solution was formed. After the addition of 3 ml (13.5 mmol) TEOS, the flask was kept for 2 hours under stirring conditions resulting in the formation of a white solution. At the same time, a mixture of HETSCH and THFPTES was made by mixing a variation of volumes of both monomers (Table 1) in a vial using a shaker. This monomer solution was subsequently added dropwise to the surfactant solution, after which the mixture was continued to be stirred for 2 more hours at room temperature. Afterward, the flask was placed in an oven where the PMO framework is aged for 48 hours at 373 K. Upon cooling down, the white solids were collected through (vacuum) assisted filtration and subsequently washed with water and ethanol. Surfactant removal was achieved by dispersing the collected residue in a flask containing 600 ml ethanol and 7 ml HCl_{aq} (37%), and leaving it to stir at room temperature for 24 hours. Upon collection of the solids through (vacuum) assisted filtration, the residue was washed extensively with ethanol until a neutral pH was reached. The solid materials were dried at 393 K under vacuum conditions (< 5 mbar), resulting in the final HR_x-THF_y-PMO materials. In this nomenclature, x and y represent the ratio of HETSCH and THFPTES respectively, added to the reaction mixture (Table 1).

2.2. Materials characterization methods

Two-dimensional transmission electron microscopy (2D TEM) pictures were taken using a JEOL JEM-1010 TEM instrument operated at 100kV without spherical aberration (Cs) correction. The powder X-ray diffraction (PXRD) pattern was measured with a Bruker D8 Advance with autochanger using Cu K-alpha irradiation with a wavelength (λ) of 0.154 nm in a Bragg-Brentano geometry. PXRD diffractograms were determined in the range of 0.2-10° with a step-size of 0.015°. The porosity of the materials was assessed through N_2-sorption, as

167 performed on a Micromeritics TriStar 3000 analyzer operated at 77 K. Prior to the analyses,
168 the samples were degassed at 393 K for 24 h. Surface areas were determined using the
169 Brunauer–Emmett–Teller (BET) method, while pore radii (r_p) were calculated using DFT
170 methods. Total pore volumes (V_{tot}) were determined at a relative pressure of $\frac{P}{P^0}$ = 0.95. A
171 Thermo Nicolet 6700 Fourier Transform IR (FT-IR) spectrometer, attached with a liquid N_2
172 cooled MCT detector was used to perform FT-IR measurements. The samples were heated to
173 393 K under vacuum, for 15 min prior to measurement. Thermogravimetric analysis (TGA)
174 was performed using a Netzsch STA 449 F3 Jupiter instrument within a temperature range of
175 293 – 1173 K under air with a heating rate of 10 K/min
176
177 2.3. Experimental apparatus and procedure
178 The schematic layout of the experimental setup is shown in Figure 1. The hydrate formation
179 tests were performed in high pressure stainless steel cylindrical reactor (effective inner volume:
180 150 cm^3, designed pressure 34.4 MPa) purchased from Swagelok (316L-50DF4-150). The high
181 pressure reactor was immersed in a mixture of water-ethylene glycol circulating bath (CORIO
182 CP-1000F, JULABO GmbH, stability: ± 0.03 K) to maintain the cold and stable temperatures
183 inside the reactor which was measured by a K-type thermocouple purchased from Testo SE &
184 Co. KGaA. The pressure in the reactor was monitored using a pressure transmitter (PAA3X-
185 30 MPa; KELLER AG für Druckmesstechnik; a range of 0-30 MPa absolute, with ± 0.01% FS
186 accuracy) for every 1 sec. H_2 gas (99.99% purity) used in this study was supplied by Air
187 Liquide Benelux Industries.
188 All the tests were performed using a standard approach as presented in earlier publications[70,
189 71], here we provide a summary of the same. Prior to the starting of experiments, the reactor
190 was thoroughly cleaned with H_2O and dried to remove any impurities. The experiments
191 commenced by adding a 1:5 ratio[69] of synthesized material (dried overnight at 348 K) to a

certain concentration of the THF solution. Subsequently, the reactor was rapidly pressurized (0.2 MPa) and depressurized with H_2 gas at least 10 times to remove any atmospheric gases. Following that, the reactor was immersed in a water-ethylene glycol bath at 298 K and gradually pressurized with H_2 gas to a predetermined initial experimental pressure of 7 MPa. These ambient thermodynamic conditions were chosen to prevent any hydrate formation and sufficient time was provided for the system to stabilize at these conditions before cooling the reactor to the experimental temperature. The experiments were considered to be complete when no significant pressure drop (0.02 MPa in 30 min) was observed due to the enclathration of H_2 gas in the hydrate cages. Each in this study was repeated two times.

At any given real-time, the amount of H_2 gas consumed during hydrate formation was quantified using the compressibility factor equation of state as shown in (Eq. 1), the normalized gas uptake (NG_t, hydrate growth) was quantified using (Eq. 2), the percentage of H_2O to hydrate conversion is determined by (Eq. 3) and (Eq. 4)

$$\Delta n_{H2,t} = V_r \left[\left(\frac{P}{zRT} \right)_{t=0} - \left(\frac{P}{zRT} \right)_t \right] \quad \text{(Eq. 1)}$$

$$NG_t = \frac{\Delta n_{H2,t}}{n_{H2O}} \ (moles\ of H_2 \ / \ moles\ of H_2O) \quad \text{(Eq. 2)}$$

$$WtH(\%) = \frac{(\Delta n_{H2,t} + \Delta n_{THF}) \times Hn}{n_{H2O}} \times 100 \quad \text{(Eq. 3)}$$

$$\Delta n_{THF} = \Delta n_{H2,t} \frac{number\ of\ large\ cages}{number\ of\ small\ cages} \quad \text{(Eq. 4)}$$

where, $\Delta n_{H2,t}$ is the moles of H_2 gas consumed at any given time t; V_r is the reactor's gas-phase volume measured using the helium expansion method[70, 71]; T and P are the temperature and pressure within the reactor; z is the compressibility of H_2 gas calculated using the Lemmon-Huber-Leachman correlation[72]; R is the ideal gas constant; n_{H2O} is the moles of H_2O introduced into the reactor; n_{THF} is the moles of THF consumed for hydrate formation with the assumption that THF occupies only the large cages of classic sII hydrate, and Hn refers to hydration number, which is considered to be 5.67 in order to comply with other binary H_2-THF hydrate experiments available in the literature[73].

The H_2 storage capacity relative to the sample's H_2O content (hydrate storage capacity: q_{H2}^{w}), H_2 capacity relative to the dry mass of the solid (dry weight storage capacity: q_{H2}^{A}), and H_2 capacity relative to the total mass of the system (total weight storage capacity: q_{H2}^{T}), were also evaluated as shown in (Eqs. 5, 6, and 7)

$$q_{H2}^{w}(wt.\%) = \frac{m_{H2}}{(m_{H2O} + m_{H2})} \times 100 \quad \text{(Eq. 5)}$$

$$q_{H2}^{A}(wt.\%) = \frac{m_{H2}}{(m_{solid} + m_{H2})} \times 100 \quad \text{(Eq. 6)}$$

$$q_{H2}^{T}(wt.\%) = \frac{m_{H2}}{m_{tot}} \times 100 \quad \text{(Eq. 7)}$$

Here, m_{H2O}, m_{solid}, and m_{H2} are masses of the H_2O, dried solid in the reactor, and quantity of enclathrated H_2 as calculated from (Eq. 1), respectively. The m_{tot} in (Eq. 7) refers to the total mass of the system, considering the mass of the dried solid, H_2O, THF, as well as the enclathrated H_2.

Another essential representation, the volumetric gas storage capacity ($\frac{volume\ of\ gas\ at\ STP}{volume\ of\ hydrate}$) was determined using (Eq. 8)[74]

230

$$Volumetric\ H_2\ storage\ capacity\left(\frac{volume\ of\ gas\ at\ STP}{volume\ of\ hydrate}\right) = K \times NG_t \qquad \text{(Eq. 8)}$$

231

$$K = \frac{v}{\frac{M_{w,hyd}}{(\rho_{hyd} \times n_{wh})}} \qquad \text{(Eq. 9)}$$

232

$$M_{w,hyd} = (136 * 18.01) + (8 * 72.11) + (16 * 2.016) \qquad \text{(Eq. 10)}$$

233

$$\rho_{hyd} = \frac{M_{w,hyd}}{(A \times \lambda^3)} \qquad \text{(Eq. 11)}$$

234 where K is the proportionality coefficient and is defined as shown in (Eq. 9), v is the volume
235 of gas at STP conditions (22.4 cm^3 $mmol^{-1}$ of gas), $M_{w,hyd}$ is molecular weight (g mol^{-1}) of sII
236 hydrate relative to the thermodynamic promoter used in this study (THF), which is calculated
237 as shown in (Eq. 10), n_{wh} is the mole of H_2O per mole of sII hydrate (i.e. 136), ρ_{hyd} (g cm^{-3})
238 is the density of hydrate, calculated using (Eq. 11), A is the Avogardo constant (6.023E23 mol^{-1})[75] and λ is the lattice parameter (17.145 Å), when THF is used as a promoter and
240 pressurized with H_2 gas[76].
241
242 3. Results and discussion
243 3.1. Material characterizations
244 The porosity of the PMO materials was assessed through N_2-sorption and the resulting
245 isotherms of the as-synthesized materials are displayed in Figure 2a. All materials exhibit a
246 type IV isotherm, characteristic of the mesoporous nature of the PMO framework. The
247 observed H_2 hysteresis loop indicates that cavitation and percolation phenomena are happening
248 during desorption, implying an inkbottle-like shape of the mesopores in the material. Compared

to HRPMO, the addition of THF-moieties in the framework initially causes a decrease in surface area by 21% (Table 2, entries 1 and 2). Upon increasing the THF content in the framework even more, a steady increase in the surface area is observed (Table 2, entries 3 and 4). This can be attributed to the incorporation of randomly organized THFPTES groups in the PMO matrix, which concurrently induces a reduction of the pore sizes of the materials (Figure 2b). These findings are corroborated through means of XRD analysis (Figure 2c) where the characteristic (100) reflection is shifted towards higher values of 2θ, demonstrating a decrease in the d-spacing of the framework (Table 2). Clear signs of the siliceous nature of the PMO materials can be recognized through FT-IR spectra (Figure 2d), owing to its typical C-H, Si-OH, and Si-O stretch vibrations at 3000-2870 cm^{-1}, 3700- 3550 cm^{-1}, and 1150-1000 cm^{-1} respectively. More careful investigation of the region of 3000-2800 cm^{-1} indicates the presence of novel organic structures in the framework, in the form of THF moieties, for the HR_x-THF_y-PMOs.

Further confirmation of the incorporation of THF-moieties was found through inspection of the TGA profiles, as displayed in Figure S1, which revealed increasing weight losses at 1173 K when larger amounts of THFPTES were added to the reaction mixture (Table 1). Upon inspection of TEM images, it is found that all PMO materials exhibit a tubular morphology with the long and short axis of the tubes ranging from 1 μm to several 100 nm respectively (Figure S2). Additionally, the tubes are found to be hollow in nature, with wall thicknesses ranging in the order of 10-30 nm. Coincidentally, when more THFPTES was added to the reaction mixture the walls become thicker as well as more disordered, substantiating the N_2 sorption and XRD results.

3.2. Effect of the framework composition on H_2 storage

To investigate the influence of THF functionalized hydrophobic porous material (HRPMO) on hydrate formation kinetics and H_2 storage capacity, a set of experiments were initially performed on non-functionalized HRPMO with stoichiometric (5.56 mol%) THF solution at temperatures ranging from 265 K to 273 K with an initial pressure of 7.0 MPa. Considering the data available in the literature[77], the equilibrium pressure of H_2-THF binary hydrate is ≈ 0.1 MPa at 277.5 K, implying that the equilibrium pressures at the temperature conditions studied in this work are expected to be less than 0.1 MPa. However, due to the unavailability of phase equilibrium data at the temperatures studied in this work, we limit ourselves to comparing the driving force with 0.1 MPa, thus the experiments performed in this work correspond to having a driving force > 6.9 MPa between equilibrium pressures at corresponding temperatures. Veluswamy and Linga[73] also reported that a driving force > 5 MPa is necessary to form a considerable amount of H_2-THF binary hydrates. Table 3. summarizes the experimental conditions, as well as H_2-THF hydrate formation results for both THF functionalized and non-functionalized HRPMO. To ensure consistency, 0.5 g of material was used in all the experiments.

Gas hydrate formation being an exothermic process, a sudden rise in sample bed temperature (measured by K-type thermocouple; Testo SE & Co. KGaA) was considered to be the onset of hydrate nucleation, followed by hydrate crystal growth, where the pressure drop observed within the reactor due to gas enclathration was translated to H_2 uptake. Figure 3 shows H_2 storage capacity in a non-functionalized HRPMO at 265 K, 269 K, and 273 K. The time zero in Figure 3 and the subsequent gas uptake Figures in this article corresponds to the onset of hydrate crystal formation (observed from the first temperature spike). As can be seen from Figure 3, a maximum H_2 storage capacity (q_{H2}^{w}) of 0.25 wt.% was achieved at 269 K; corresponding to 22.74 mmol H_2/mol H_2O, followed by a decrease in storage capacity as temperature increased. On the other hand, the three gas uptake curves at different temperatures

298 also demonstrate the consistency of hydrate formation with a minor standard deviation. It can
299 also be seen that the H_2 uptake plateaus off at ≈ 40 min after nucleation, with 80% of maximum
300 storage capacity achieved in ≈ 8 min, 9 min, and 16.5 min at 265 K, 269 K, and 273 K
301 respectively.

302 Figures 4a, 4b, and 4c exhibit the H_2 storage capacities of THF-like functionalized HRPMO
303 materials at three different temperatures. The hydrate growth curves show good consistency
304 across the board, as seen by minimal standard deviations. As can be observed, the gas uptake
305 curves show a significant increase before it reaches a plateau, and altering the proportion of
306 these functionalities on the HRPMO produced substantial results in H_2 uptake (Table 3), with
307 HR_{95}-THF_5-PMO outperforming HR_{80}-THF_{20}-PMO followed by HR_{50}-THF_{50}-PMO at all
308 temperatures studied. For instance, at the lowest temperature of 265 K, HR_{95}-THF_5-PMO
309 attained a maximum H_2 storage capacity of 0.26 wt.%, which is ≈ 13.6% and 21% higher than
310 that of HR_{80}-THF_{20}-PMO and HR_{50}-THF_{50}-PMO, respectively. These results also imply that
311 higher amounts of THF-like functionalities added to HRPMO induce a reduction of final H_2
312 uptake. The H_2 storage capacity at different temperatures for respective materials is shown in
313 Figure S3. Another noteworthy effect of the surface chemistry tuning of the materials lies in
314 the time required to form the H_2 clathrates. It was found that the presence of surface-bound
315 THF-like moieties could significantly stimulate clathrate formation, with the effect becoming
316 more pronounced at higher temperatures (Figure 5). A comparison of the clathrate formation
317 performances at 273 K of non-functionalized HRPMO and HR_{95}-THF_5-PMO demonstrates that
318 the THF-like moieties could enhance the hydrate growth kinetics (time required to reach 80%
319 of maximum storage capacity) by at least 28%.

320 Furthermore, Figure 5 shows the H_2 gas uptake (hydrate growth) curves in non-
321 functionalized HRPMO and HR_{95}-THF_5-PMO, and as can be seen, the materials tunned with
322 THF-like functionalities exhibit relatively higher (at least 3%, inclusive of standard deviation)

323 H_2 gas uptake than HRPMO at all temperatures. These findings unequivocally indicate that the
324 solid-state tunning of the material with the promoter (THF) molecule-like functional groups
325 can improve overall H_2 storage capacities rather than tuning the THF concentration in the
326 solution as reported by Lee et al.[37], which is still being debated. To corroborate the
327 suggestion from Lee et al[37], the non-functionalized HRPMO and HR_{95}-THF_5-PMO were
328 also tested with 0.1 and 0.3 mol% THF solution, however, no clathrate formation was observed
329 at 265 K for a period of 12 hrs.
330 Based on previous literature reports on hydrophobic porous materials for H2-THF clathrate
331 formation, a following mechanistic hypothesis could be drawn for the HRPMO and HRx-
332 THFy-PMO materials. While pristine HRPMO has been demonstrated to be hydrophobic, due
333 to the organic nature of the utilized organosilica monomer[69], it still shows some degree of
334 hydrophilicity due to the presence of Si-OH functionalities throughout the surface. The
335 integration of THF-like moieties on the surface of the HR_x-THF_y-PMO on the other hand
336 further enhances the hydrophobicity of the porous structure compared to the HRPMO. The
337 degree of surface hydrophobicity has been shown to influence clathrate formation in two major
338 ways[59, 65], as depicted in Figure 6. Hydrophilic surfaces tend to form a structured
339 organization of water molecules near the surface, known as non-freezable water causing high
340 energy requirements to form ice structures. Hydrophobic surfaces tend to perturb the structural
341 organization of the otherwise strongly ordered surface bound water, lowering the energy
342 requirements necessary to reorganize water molecules towards other crystalline structures
343 (Figure 6, left). The second major influence results from the increase in the concentration of
344 adsorbed gas-molecules (H_2 in this work) on the hydrophobic surface (Figure 6, right). This
345 gas-enriched layer on the surface of the porous medium increases the driving force of clathrate
346 formation, significantly stimulating the formation kinetics.

It is scientifically known that pure H_2-H_2O forms sII hydrate at extremely high pressures and can yield a maximum H_2 storage capacity of 5.6 wt.% if both small and large cages occupy 2 and 5 H_2 molecules, respectively[30, 78] (a probable theoretical maximum H_2 storage capacities in sII hydrate are presented in Table 2). On the other hand, when THF (thermodynamic promoter) is added to H_2O in stoichiometric concentrations, the H_2 can only occupy small cages, leaving large cages for THF, resulting in an overall decreased storage capacity of 1.3 wt.%, when occupied by 1 H_2 molecule and 2.5 wt.% when occupied by 2 H_2 molecules. However, as can be seen from Table 3, in an H_2-promoter (stoichiometric conc.)-H_2O system at different thermodynamic conditions, the maximum H_2 storage capacity is < 1.3 wt.% indicating that the fractional H_2 occupancy in small cages is less than 1 or not all small (5^{12}) cages are filled at those conditions, which on the other hand can be enhanced by increasing the pressure of the system. Table 3 also shows that solid state tunning of the material can improve the H_2 storage capacity by enclathrating more H_2 molecules in 5^{12} cages at relatively low pressures as compared to literature. Although powder-THF hydrate shows better H_2 enclathration, it is to be noted that the fine THF hydrate particles relapse to liquid phase upon melting which is not compatible with continuous cycles.

4. Conclusion

H_2 storage in the form of clathrate hydrates, while being an attractive alternative to compression or liquefaction, remains an energetically intensive process. Additives such as THF have been extensively applied to reduce the necessary energy input in the form of lowered formation pressures and milder temperatures. Nevertheless, the constraints on mass transfer rate and enclathration kinetics in bulk systems have been hampering the advancement of this technology. To this end, unstirred systems coupled with hydrophobic porous materials are being explored due to their ease of handling, recyclability, and potential to accelerate the

kinetics of hydrate formation. In this study, hydrophobic Hollow Ring-PMO (HRPMO) nanoparticles with a variation in the concentration of surface-bound THF-like moieties were designed as a novel additive for enhanced H_2 clathrate formation. Their performance was assessed under the stoichiometric concentration of THF solution at 7 MPa in a range of different temperatures (265 K, 269 K, and 273 K) using a volumetric approach. The results revealed that THF-functionalized HRPMO significantly accelerated clathrate formation, reducing the time to reach maximum storage capacity by up to 28%, especially at higher temperatures when compared with non-functionalized HRPMO. Despite having lower surface area and pore volume than the non-functionalized HRPMO, a 3% increase in H_2 storage capacity (inclusive of standard deviation) equating to 0.26 wt.% at lower temperature was observed when 0.14 mmol/g of the promoter was incorporated in the framework. A similar trend in H_2 uptake was observed even at other temperatures studied in this work. On the other hand, higher loadings of promotor agent resulted in a considerable reduction in storage capacities. These findings emphasize the significance of tuning the porous materials with THF-like moieties for higher gas storage capacities and these findings resemble previously reported cases that expressed the dependence of H_2 storage capacities on the THF concentrations in H_2-THF binary clathrates. However, to the best of our knowledge, this is the first report where such a solid-state storage capacity tuning effect is observed using solid additives for H_2 clathrate formation. These findings substantiate the importance of carefully fine-tuning the surface chemistry of additives for clathrate formation and help further pave the way towards industrially viable H_2 storage in the form of clathrate hydrates. In conclusion, it is also strongly recommended to undertake a comprehensive molecular-level investigation in order to attain a more profound understanding of the solid-state tuning effects on supporting materials and their role in augmenting H_2 storage capacities.

CRediT authorship contribution statement

Geert Watson: Writing – review & editing, Writing – original draft, Methodology, Formal analysis, Conceptualization. **Nithin B. Kummamuru**: Writing – review & editing, Writing – original draft, Methodology, Formal analysis, Conceptualization. **Pascal Van Der Voort**: Writing – review & editing, Supervision, Methodology, Funding acquisition, Conceptualization. **Sammy W. Verbruggen**: Supervision, Funding acquisition. **Patrice Perreault**: Writing – review & editing, Supervision, Methodology, Funding acquisition, Conceptualization.

Acknowledgment

All authors acknowledge VLAIO for Moonshot funding (ARCLATH, n° HBC.2019.0110, ARCLATH2, n° HBC.2021.0254). PVDV acknowledges UGent for BOFBAS2020000401 for the funding of the XRD diffractometer.

Corresponding author*
pascal.vandervoort@ugent.be Tel:
ORCID

Notes

The authors declare no competing financial interest.

Supporting Information

The supporting information is available free of charge on the Publications website at DOI:

Table 1. Quantity of the added organosilanes in the HR_x-THF_y-PMO synthesis

Sample	V_{HETSCH} (ml) n_{HETSCH} (mmol)	$V_{THFPTES}$ (ml) $n_{THFPTES}$ (mmol)
HRPMO	3 8.24	/
HR_{95}-THF_5-PMO	2.85 7.83	0.15 0.48
HR_{80}-THF_{20}-PMO	2.4 6.59	0.6 1.94
HR_{50}-THF_{50}-PMO	1.5 4.12	1.5 4.85

Table 2. Overview of the characteristics of the PMO materials.

Entry	Sample	THFPTES loading (mmol/g)[a]	S_{BET}(m²/g)	V_{tot} (cm³/g)[b]	r_p (nm)[c]	d-spacing (nm)[d]
1	HRPMO	/	790	0.90	1.89	5.04
2	HR_{95}-THF_5-PMO	0.14	620	0.56	1.77	5.01
3	HR_{80}-THF_{20}-PMO	0.48	650	0.85	1.65	4.47
4	HR_{50}-THF_{50}-PMO	1.11	850	0.71	1.29	3.88

[a] Determined using TGA profiles between 200-900°C; [b] Determined at P/P°=0.95; [c] Determined using a NLDFT method assuming a silica matrix exhibiting cylindrical pores on the adsorption branch with relative fitting errors <1%; [d] Determined using Bragg's law with λ=0.154 nm)

Table 3. Summary of H_2 storage capacities in H_2/THF(5.56 mol%)/H_2O system in functionalized and non-functionalized HRPMO at different thermodynamic conditions

System	P (MPa)	T (K)	NG_t (moles H_2/moles H_2O)	WtH (%)	q^{w}_{H2} (wt.%)	q^{A}_{H2} (wt.%)	q^{T}_{H2} (wt.%)	Volumetric H_2 storage (v/v)
Non-functionalized HRPMO	7	265	22.75	19.35	0.254	1.042	0.205	22.83
	7	269	20.55	17.46	0.229	0.941	0.185	20.61
	7	273	19.38	16.48	0.216	0.889	0.174	19.45
HR_{95}-THF_5-PMO	7	265	23.61	20.08	0.264	1.081	0.212	23.70
	7	269	21.53	18.31	0.240	0.986	0.194	21.61
	7	273	20.08	17.09	0.224	0.921	0.181	20.17
HR_{80}-THF_{20}-PMO	7	265	20.77	17.68	0.232	0.952	0.187	20.85
	7	269	19.45	16.54	0.217	0.892	0.175	19.53
	7	273	17.51	14.89	0.196	0.804	0.158	17.58
HR_{50}-THF_{50}-PMO	7	265	19.49	16.59	0.218	0.895	0.176	19.58
	7	269	18.21	15.49	0.203	0.836	0.164	18.28
	7	273	16.52	14.05	0.185	0.759	0.149	16.59

Table 4. Theoretical storage capacity of H_2 in sII hydrate cages

System	Small cage (5^{12})	Large cage ($5^{12}6^4$)	H_2 storage capacity (wt.%)
H_2-H_2O	1	1	1.94
	1	2	2.56
	1	3	3.19
	1	4	3.80
	1	5	4.40
	2	1	3.18
	2	2	3.80
	2	3	4.40
	2	4	5.00
	2	5	5.60
H_2-THF-H_2O	1	0	1.30
	2	0	2.56

Table 5. H_2 storage capacity in sII hydrates below 15 MPa using promoters (stoichiometric conc.)

System	P (MPa)	T (K)	H_2 storage capacity (wt.%)	Occupancy of 5^{12} cages* (%)	Ref.
THF in Porous media (HR_{95}-THF_5-PMO)	7.0	265	0.26	10.05	This work
	7.0	269	0.24	9.14	
	7.0	273	0.22	8.37	
THF-Bulk solution/stirring	13	279.2	0.183	6.96	[79]
DIOX-Bulk solution/stirring	12.3	271.15	0.216	8.22	[74]
THF in Porous media	11.6	270	0.4	15.25	[55]
Powdered DXN hydrate	12.0	233	0.4	15.25	[80]
ECP-Bulk solution	12.2	273.25	0.310	11.81	[53]
THF-Bulk solution/stirring	7.0	278.2	0.14	5.25	[73]
	5.0	278.2	0.12	4.40	
	5.0	278.2	0.13	4.76	
	5.0	278.2	0.10	3.92	
Powdered THF hydrate	5.0	265.1	0.18	6.85	[81]
	5.0	269	0.16	6.10	
	5.0	273.2	0.15	5.71	
Powdered THF hydrates	6.5	269.5	0.23	8.75	[82]
	6.5	269.5	0.23	8.75	
	6.5	269.5	0.20	7.61	
	8.4	269.5	0.25	9.52	
	6.5	269.5	0.23	8.75	
	3.6	269.5	0.19	7.23	
	6.5	266.7	0.26	9.90	
	6.5	269.5	0.23	8.75	
	6.5	275.1	0.21	7.99	

Powdered THF hydrate	6.7	270	0.36	13.63	[40]
	12.2		0.46	17.70	
	6.2		0.38	14.56	
	12.1		0.55	21.13	
	12.4		0.32	12.28	
Powdered THF hydrates	10.7	277.15	0.19	7.23	[52]
	11.4		0.26	9.90	

*Considering two H_2 molecules in a single small cage

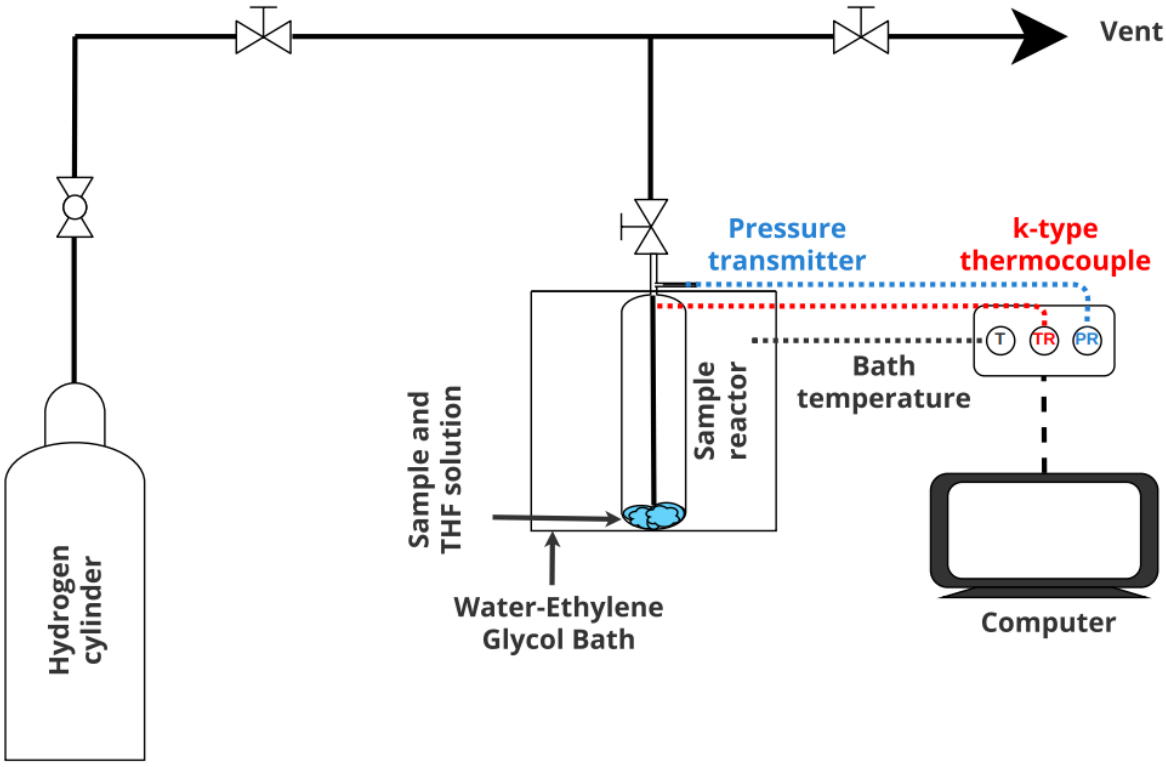

Figure 1. The schematic of the experimental setup for the study of binary H_2-THF hydrate formation in HRPMO

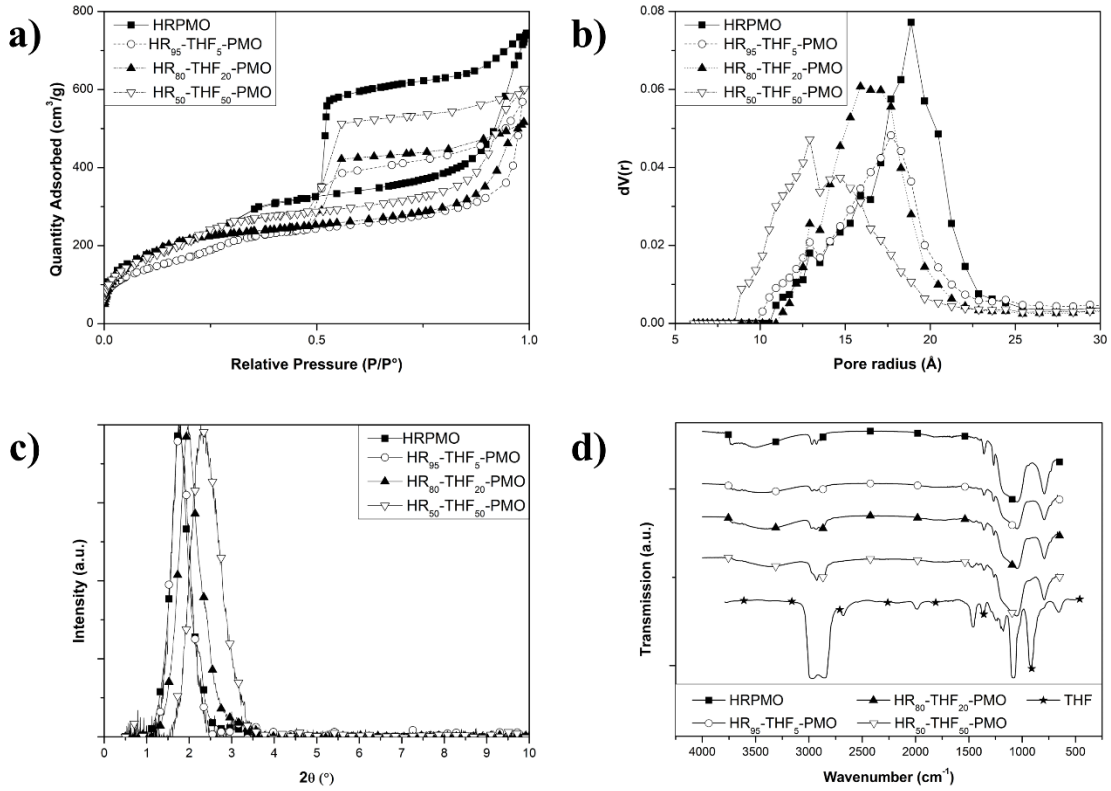

Figure 2. Overview of the characteristics of the PMO materials: a) N_2 sorption isotherms, b) DFT calculated pors size distributions, c) XRD diffractograms, d) FTIR spectra.

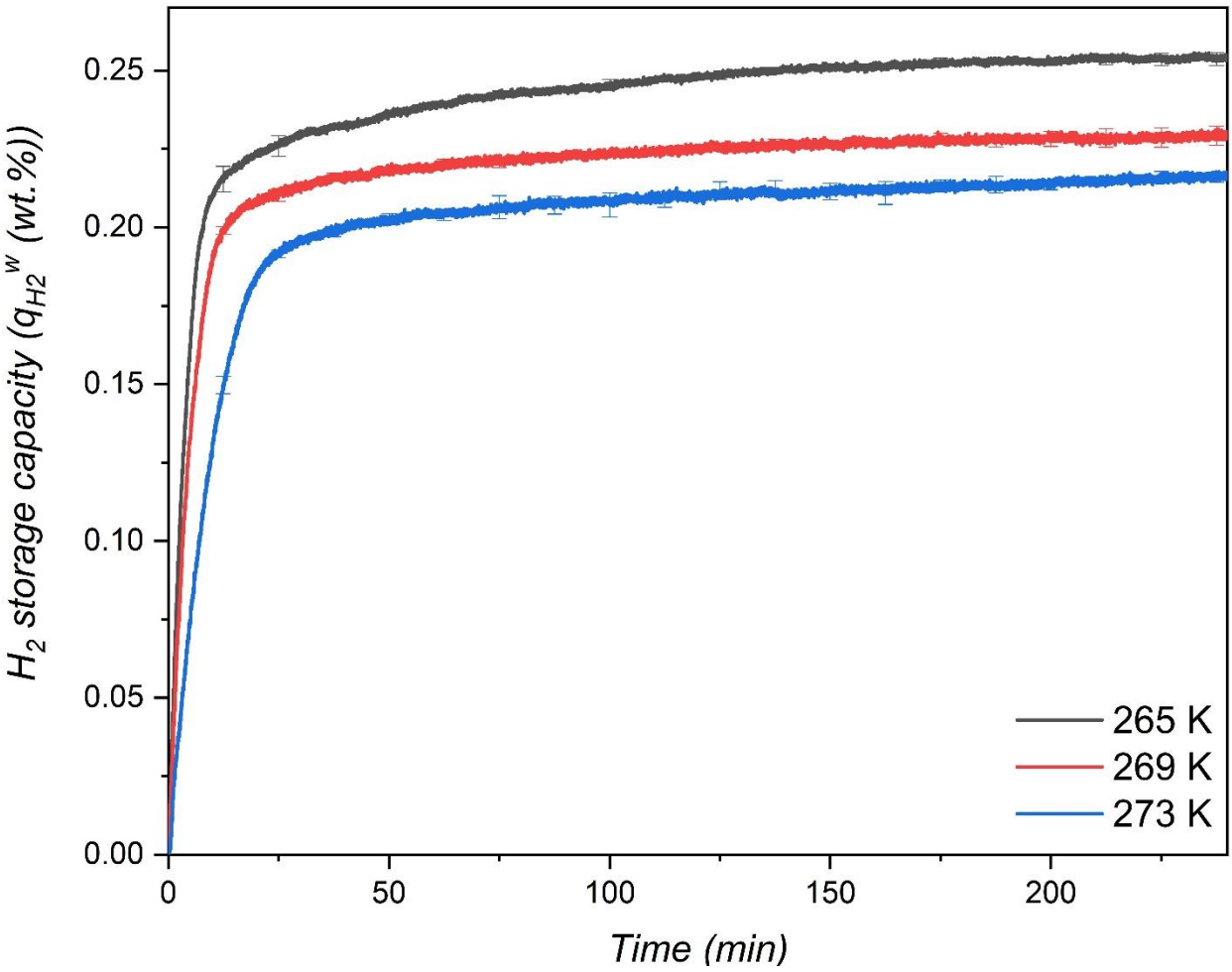

Figure 3. H_2 storage capacity at three different temperatures in non-functionalized HRPMO

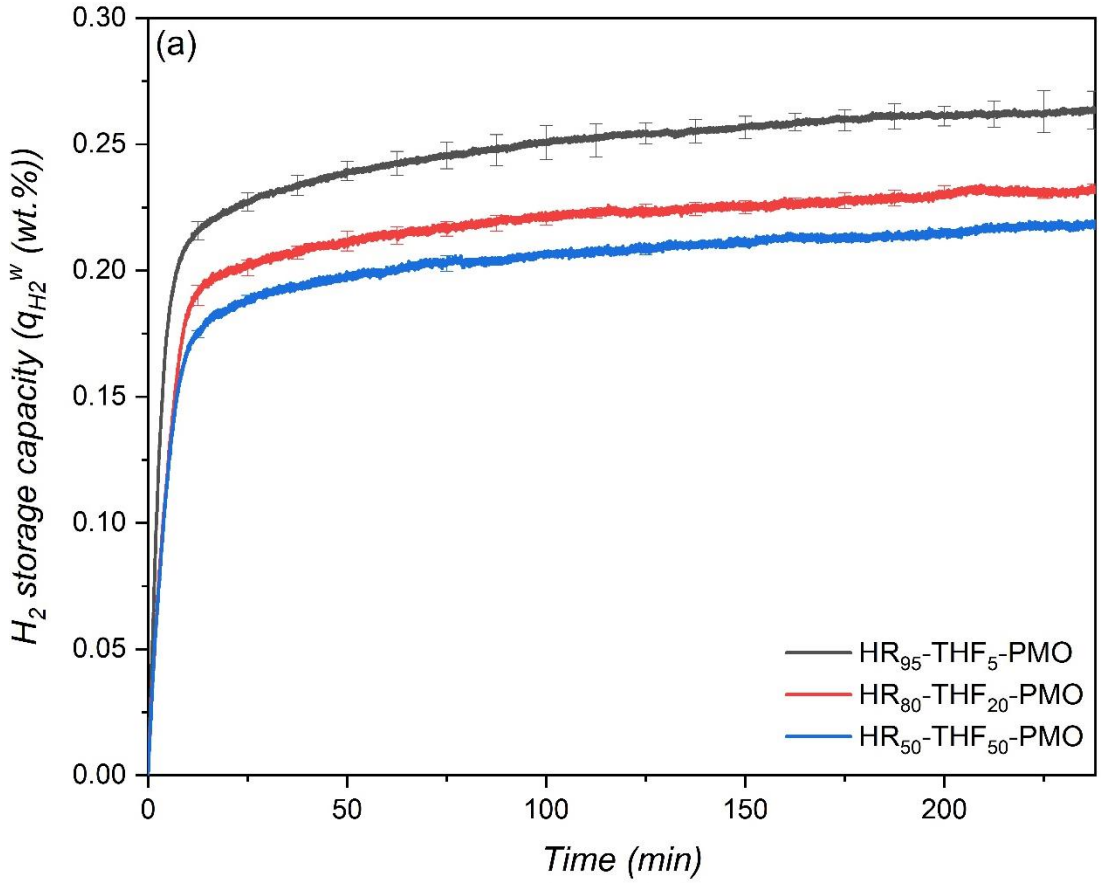
(a)
0.30
0.25
0.20
0.15
0.10
0.05
0.00
0
50
100
150
200
Time (min)
H2 storage capacity (qH2w (wt.%))
HR95-THF5-PMO
HR80-THF20-PMO
HR50-THF50-PMO

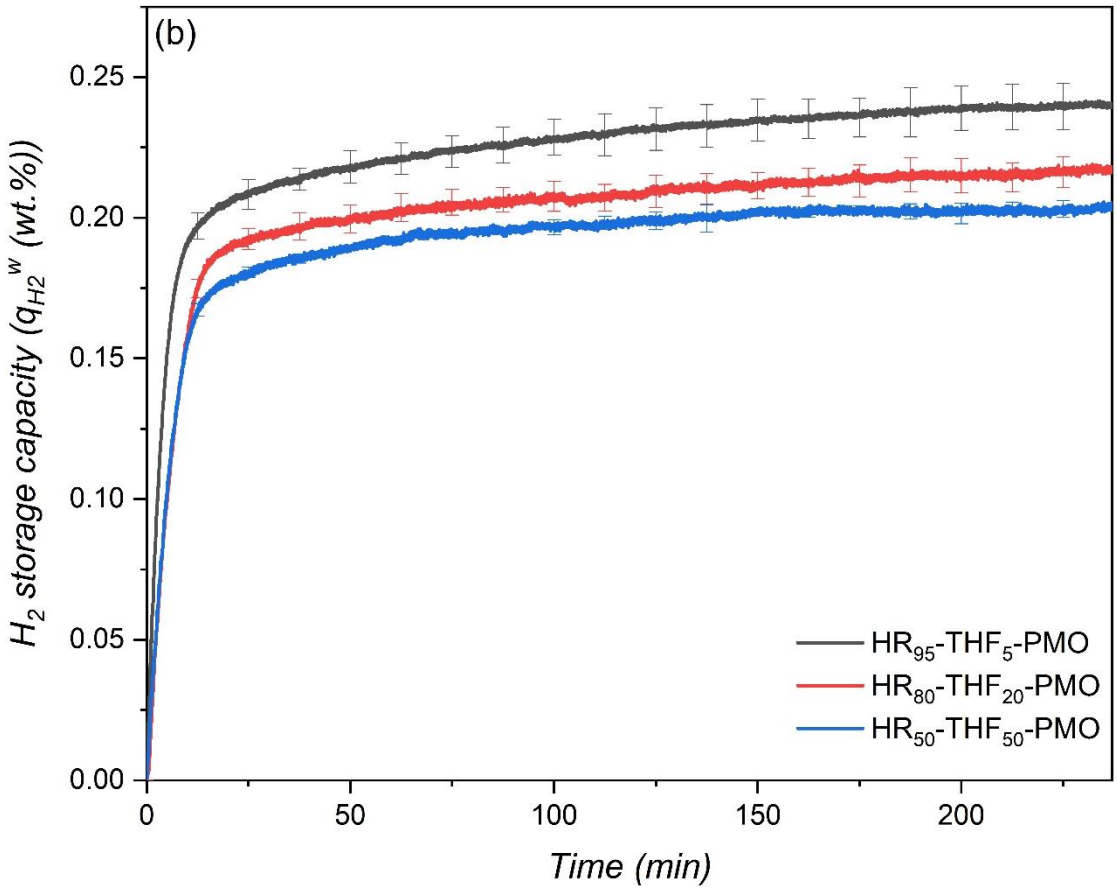
(b)
0.25
0.20
0.15
0.10
0.05
0.00
0
50
100
150
200
Time (min)
H2 storage capacity (qH2w (wt.%))
HR95-THF5-PMO
HR80-THF20-PMO
HR50-THF50-PMO

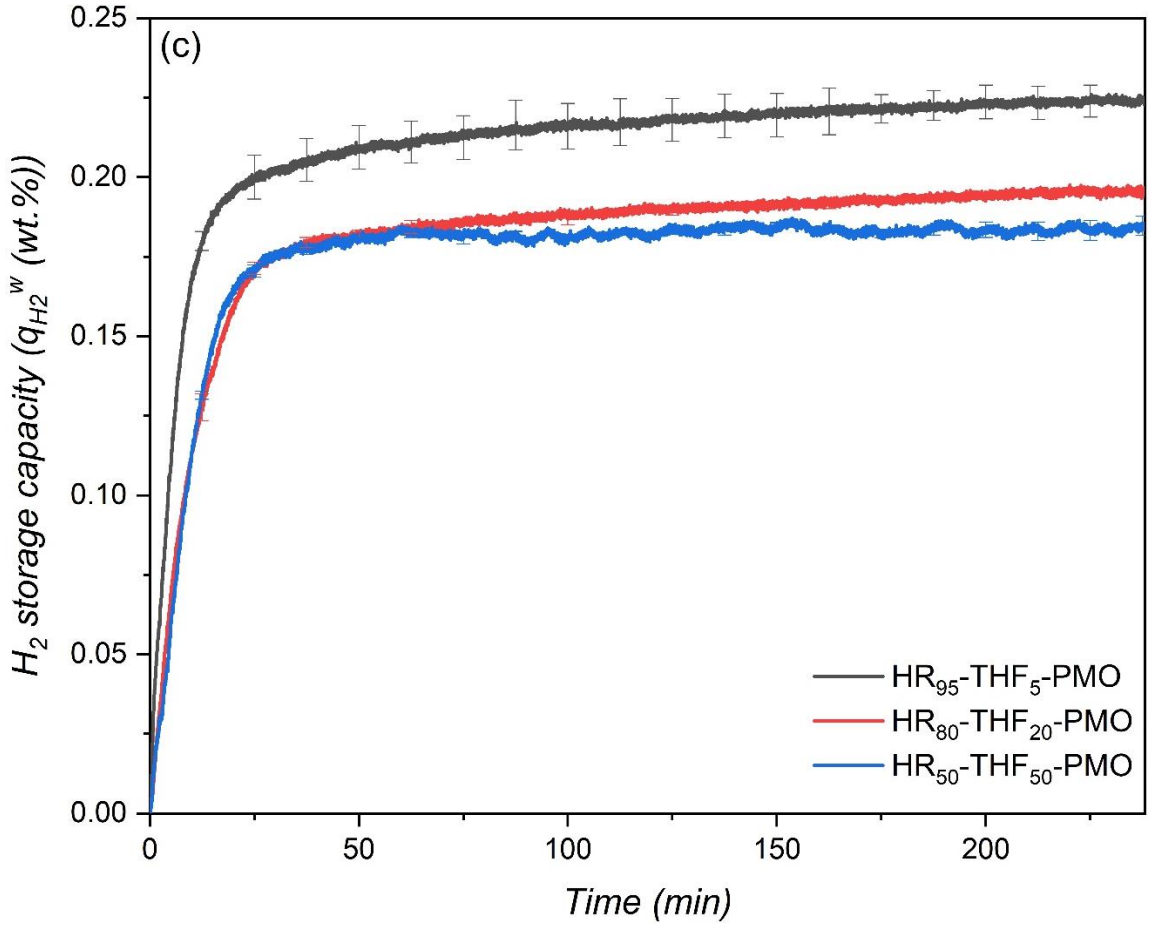

Figure 4. H_2 storage capacities in three different THF-like functionalized materials at three different temperatures; (a): 265 K, (b): 269 K, (c): 273 K

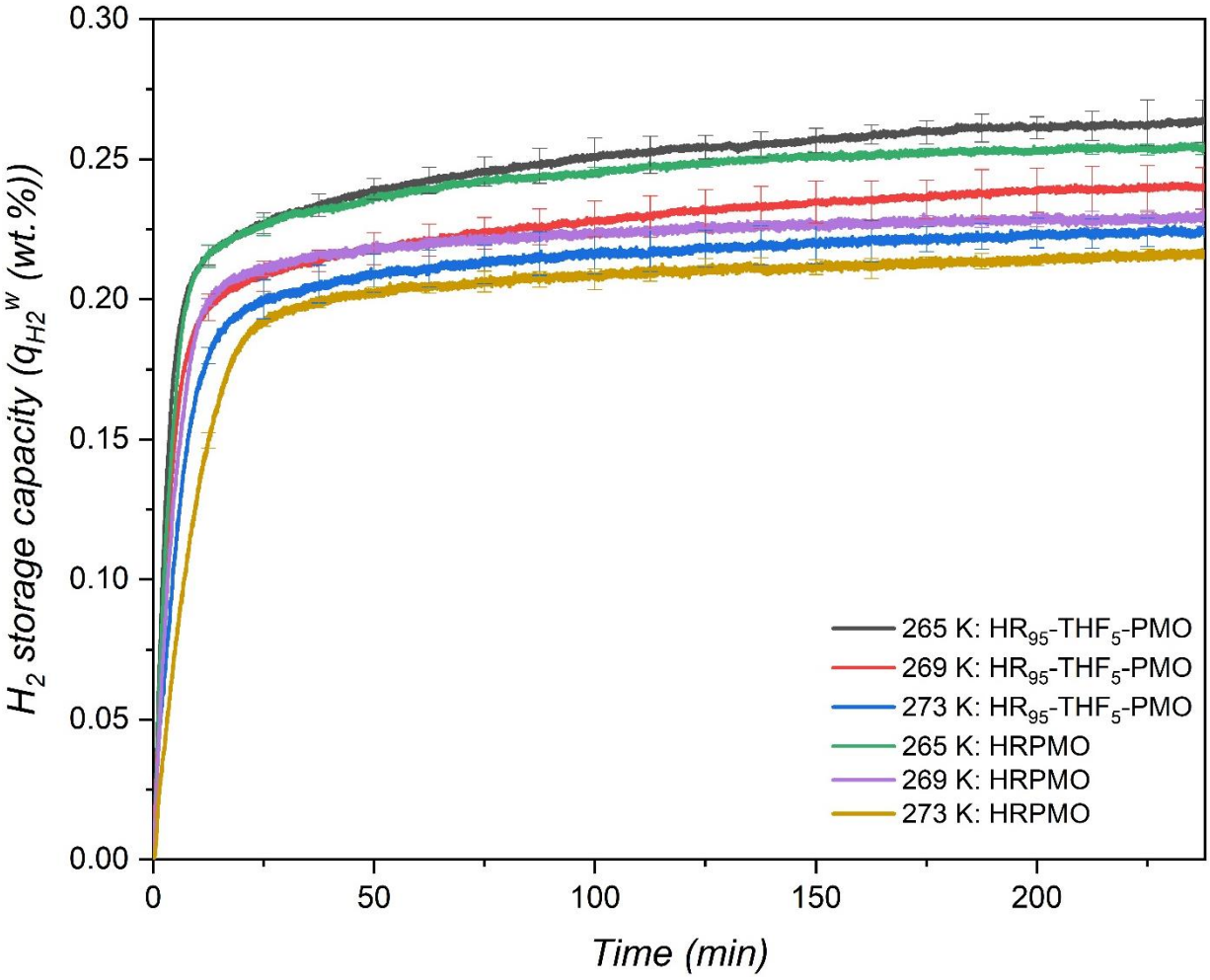

Figure 5. H_2 gas uptake (hydrate growth) curves in non-functionalized HRPMO and HR_{95}-THF_5-PMO at different temperatures

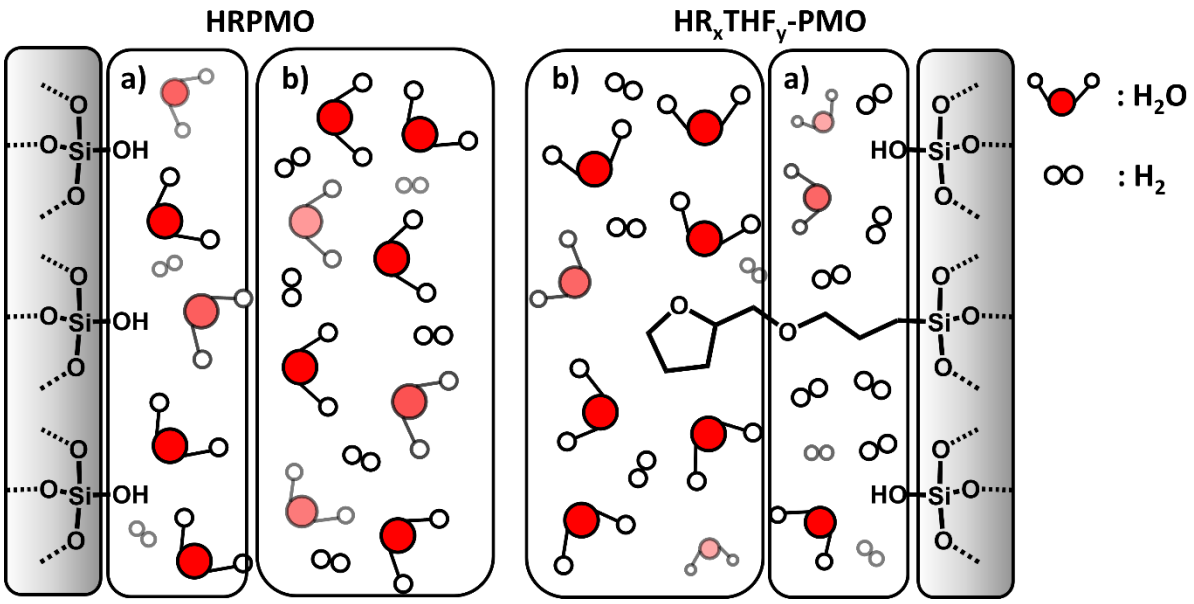

Figure 6: Depiction of clathrate formation mechanisms in HRPMO (left) versus HR_x-THF_y-PMO (right).

References

[1] E. Tzimas, C. Filiou, S. D. Peteves, J. B. Veyre, Hydrogen storage: State-of-the-art and future perspective, Netherlands, 2003,

[2] IEA, Global hydrogen review 2022, Paris, 2022, https://www.iea.org/reports/global-hydrogen-review-2022

[3] IEA, Hydrogen, Paris, 2022, https://www.iea.org/reports/hydrogen

[4] M. Hirscher, Handbook of hydrogen storage: New materials for future energy storage, Wiley-VCH Verlag GmbH & Co. KGaA, Weinheim, Germany, 2010.

[5] H. Barthélémy, M. Weber, F. Barbier, Hydrogen storage: Recent improvements and industrial perspectives, Int. J. Hydrogen Energy 42 (2017) 7254-7262.

[6] R. S. Irani, Hydrogen storage: High-pressure gas containment, MRS Bulletin 27 (2002) 680-682.

[7] A. Züttel, Materials for hydrogen storage, Mater. Today 6 (2003) 24-33.

[8] V. V. Struzhkin, B. Militzer, W. L. Mao, H-K. Mao, R. J. Hemley, Hydrogen storage in molecular clathrates, Chem. Rev. 107 (2007) 4133-4151.

[9] M. Mohan, V. K. Sharma, E. A. Kumar, V. Gayathri, Hydrogen storage in carbon materials—A review, Energy storage 1 (2019) e35.

[10] D. Zhao, X. Wang, L. Yue, Y. He, B. Chen, Porous metal–organic frameworks for hydrogen storage, Chem. Commun. 58 (2022) 11059-11078.

[11] L. Zhang, M. D. Allendorf, R. Balderas-Xicohténcatl, D. P. Broom, G. S. Fanourgakis, G. E. Froudakis, T. Gennett, K. E. Hurst, S. Ling, C. Milanese, P. A. Parilla, D. Pontiroli, M. Riccò, S. Shulda, V. Stavila, T. A. Steriotis, C. J. Webb, M. Witman, M. Hirscher, Fundamentals of hydrogen storage in nanoporous materials, Prog. Energy 4 (2022) 042013.

[12] Á. Berenguer-Murcia, J. P. Marco-Lozar, D. Cazorla-Amorós, Hydrogen storage in porous materials: Status, Milestones, and Challenges, Chem. Rec. 18 (2018) 900-912.

[13] Z. Chen, K. O. Kirlikovali, K. B. Idrees, M. C. Wasson, O. K. Farha, Porous materials for hydrogen storage, Chem 8 (2022) 693-716.

[14] K. M. Thomas, Hydrogen adsorption and storage on porous materials, Catal. Today 120 (2007) 389-398.

[15] M. Pumera, Graphene-based nanomaterials for energy storage, Energy Environ. Sci. 4 (2011) 668-674.

[16] E. Rivard, M. Trudeau, K. Zaghib, Hydrogen storage for mobility: A review, Materials 19 (2019) 1973.

[17] N. A. A. Rusman, M. Dahari., A review on the current progress of metal hydrides material for solid-state hydrogen storage applications, Int. J. Hydrogen Energy 41 (2016) 12108-12126.

[18] B. Sakintuna, F. Lamari-Darkrim, M. Hirscher, Metal hydride materials for solid hydrogen storage: A review, Int. J. Hydrogen Energy 32 (2007) 1121-1140.

[19] P. Modi, K. F. Aguey-Zinsou, Room temperature metal hydrides for stationary and heat storage applications: A review, Front. Energy Res. 9 (2021).

[20] J. Graetz, New approaches to hydrogen storage, Chem. Soc. Rev. 38 (2009) 73-82.

[21] F. Schuth, B. Bogdanovic, M. Felderhoff, Light metal hydrides and complex hydrides for hydrogen storage, Chem. Commun. (2004) 2249-2258.

[22] R. B. Biniwale, S. Rayalu, S. Devotta, M. Ichikawa, Chemical hydrides: a solution to high capacity hydrogen storage and supply, Int. J. Hydrogen Energy 33 (2008) 360-365.

[23] C. Chu, K. Wu, B. Luo, Q. Cao, H. Zhang, Hydrogen storage by liquid organic hydrogen carriers: Catalyst, renewable carrier, and technology – A review, Carbon Resour. Convers. 6 (2023) 334-351.
[24] M. Aziz, A. T. Wijayanta, A. B. D. Nandiyanto, Ammonia as Effective Hydrogen Storage: A Review on Production, Storage and Utilization, Energies 13 (2020) 3062.
[25] H. W. Langmi, N. Engelbrecht, P. M. Modisha, D. Bessarabov, Chapter 13 - Hydrogen storage, in: T. Smolinka, J. Garche, (Eds.), Electrochemical Power Sources: Fundamentals, Systems, and Applications, Elsevier, 2022, pp. 455-486.
[26] H. Q. Nguyen, B. Shabani, Review of metal hydride hydrogen storage thermal management for use in the fuel cell systems, Int. J. Hydrogen Energy 46 (2021) 31699-31726.
[27] P. Perreault, L. V. Hoecke, H. Pourfallah, N. B. Kummamuru, C.-R. Boruntea, P. Preuster, Critical challenges towards the commercial rollouts of a LOHC-based H_2 economy, Curr. Opin. Green Sustain. Chem. 41 (2023) 100836.
[28] S. Chatterjee, R. K. Parsapur, K.-W. Huang, Limitations of Ammonia as a Hydrogen Energy Carrier for the Transportation Sector, ACS Energy Lett. 6 (2021) 4390-4394.
[29] Y. A. Dyadin, E. G. Larionov, A. Y. Manakov, F. V. Zhurko, E. Y. Aladko, T. V. Mikina, V. Y. Komarov, Clathrate hydrates of hydrogen and neon, Mendeleev Commun. 5 (1999) 209-210.
[30] W. L. Mao, H. K. Mao, A. F. Goncharov, V. V. Struzhkin, Q. Z. Guo, J. Z. Hu, J. F. Shu, M.S. R. J. Hemley, Y. S. Zhao, Hydrogen clusters in clathrate hydrate, Science 297 (2002) 2247-2249.
[31] L. J. Florusse, C. J. Peters, J. Schoonman, K. C. Hester, C. A. Koh, S. F. Dec, K. N. Marsh, E. D. Sloan, Stable low-pressure hydrogen clusters stored in a binary clathrate hydrate, Science 306 (2004) 469-471.
[32] E. D. Sloan, C. A. Koh, Clathrate hydrates of natural gases, 3 ed., Taylor & Francis-CRC Press, Boca Raton, FL, 2008.
[33] W. L. Vos, L. W. Finger, R. J. Hemley, H-k. Mao, Novel H_2-H_2O clathrates at high pressures, Phys. Rev. Lett. 71 (1993) 3150-3153.
[34] Y. A. Dyadin, E. G. Larionov, E. Y. Aladko, A. Y. Manakov, F. V. Zhurko, T. V. Mikina, V. Y. Komarov, E. V. Grachev, Clathrate formation in water-noble gas (hydrogen) systems at high pressures J. Struct. Chem. 40 (1999) 790-795.
[35] K. A. Lokshin, Y. Zhao, D. He, W. L. Mao, H-K. Mao, R. J. Hemley, M. V. Lobanov, M. Greenblatt, Structure and dynamics of hydrogen molecules in the novel clathrate hydrate by high pressure neutron diffraction, Phys. Rev. Lett. 93 (2004) 125503.
[36] S. Patchkovskii, J. S. Tse, Thermodynamic stability of hydrogen clathrates, PNAS 100 (2003) 14645-14650.
[37] H. Lee, J.-W. Lee, D. Y. Kim, J. Park, Y. T. Seo, H. Zeng, I. L. Moudrakovski, C. I. Ratcliffe, J. A. Ripmeester, Tuning clathrate hydrates for hydrogen storage, Nature 434 (2005) 743-746.
[38] D-Y. Kim, Y. Park, H. Lee, Tuning clathrate hydrates: Application to hydrogen storage, Catal. Today 120 (2007) 257-261.
[39] R. Anderson, A. Chapoy, B. Tohidi, Phase relations and binary clathrate hydrate formation in the system H_2-THF-H_2O, Langmuir 23 (2007) 3440-3444.
[40] T. A. Strobel, C. J. Taylor, K. C. Hester, S. F. Dec, C. A. Koh, K. T. Miller, E. D. Sloan, Molecular hydrogen storage in binary THF−H2 clathrate hydrates, J. Phys. Chem. B 110 (2006) 17121-17125.
[41] N. I. Papadimitriou, I. N. Tsimpanogiannis, A. Th. Papaioannou, A. K. Stubos, Evaluation of the hydrogen-storage capacity of pure H2 and binary H2-THF hydrates with monte carlo simulations, J. Phys. Chem. C 112 (2008) 10294-10302.

[42] S. Hashimoto, T. Sugahara, H. Sato, K. Ohgaki, Thermodynamic Stability of H2 + tetrahydrofuran mixed gas hydrate in nonstoichiometric aqueous solutions, J. Chem. Eng. Data 52 (2007) 517-520.
[43] A. Gupta, G. V. Baron, P. Perreault, S. Lenaerts, R-G. Ciocarlan, P. Cool, P. G. M. Mileo, S. Rogge, V. V. Speybroeck, G. Watson, P. V. D. Voort, M. Houlleberghs, E. Breynaert, J. Martens, J. F. M. Denayer, Hydrogen clathrates: Next generation hydrogen storage materials, Energy Storage Mater. 41 (2021) 69-107.
[44] H. P. Veluswamy, R. Kumar, P. Linga, Hydrogen storage in clathrate hydrates: Current state of the art and future directions, Appl. Energy 122 (2014) 112-132.
[45] H. P. Veluswamy, W. J. Ang, D. Zhao, P. Linga, Influence ofcationic and non-ionic surfactants on the kinetics of mixed hydrogen/tetrahydrofuran hydrates, Chem. Eng. Sci. 132 (2015) 186-199.
[46] A. Lokshin, Y. Zhao, Fast synthesis method and phase diagram of hydrogen clathrate hydrate, Appl. Phys. Lett. 88 (2006) 131909.
[47] S. Alavi, J. A. Ripmeester, Hydrogen-gas migration through clathrate hydrate cages, Angew. Chem. Int. Ed. 46 (2007) 6102-6105.
[48] P. Englezos, Nucleation and growth of gas hydrate crystals in relation to kinetic inhibition, Rev IFP 51 (1996) 789.
[49] F. Rossi, M. Filipponi, B. Castellani, Investigation on a novel reactor for gas hydrate production, Appl. Energy 99 (2012) 167-172.
[50] A. Vysniauskas, P.R. Bishnoi, A kinetic study of methane hydrate formation, Chem. Eng. Sci. 38 (1983) 1061-1072.
[51] A. Talyzin, Feasibility of H2–THF–H2O clathrate hydrates for hydrogen storage applications, Int. J. Hydrogen Energy 33 (2008) 111-115.
[52] K. Ogata, S. Hashimoto, T. Sugahara, M. Moritoki, H. Sato, K. Ohgaki, Storage capacity of hydrogen in tetrahydrofuran hydrate, Chem. Eng. Sci. 63 (2008) 5714-5718.
[53] S. Chen, Y. Wang, X. Lang, S. Fan, G. Li, Rapid and high hydrogen storage in epoxycyclopentane hydrate at moderate pressure, Energy 268 (2023) 126638.
[54] F. Su, C. L. Bray, B. O. Carter, G. Overend, C. Cropper, J. A. Iggo, Y. Z. Khimyak, A. M. Fogg, A.I. Cooper, Reversible hydrogen storage in hydrogel clathrate hydrates, Adv. Mater. 21 (2009) 2382-2386.
[55] F. Su, C. L. Bray, B. Tan, A. I. Cooper, Rapid and reversible hydrogen storage in clathrate hydrates using emulsion-templated polymers, Adv. Mater. 20 (2008) 2663-2666.
[56] D. Saha, S. Deng, Accelerated Formation of THF-H2 Clathrate Hydrate in Porous Media, Langmuir 26 (2010) 8414-8418.
[57] D. Saha, S. Deng, Enhanced hydrogen adsorption in ordered mesoporous carbon through clathrate formation, Int. J. Hydrogen Energy 34 (2009) 8583-8588.
[58] J. Farrando-Perez, R. Balderas-Xicohtencatl, Y. Cheng, L. Daemen, C. Cuadrado-Collados, M. Martinez-Escandell, A. J. Ramirez-Cuesta, J. Silvestre-Albero, Rapid and efficient hydrogen clathrate hydrate formation in confined nanospace, Nature 13 (2022) 5953.
[59] M. E. Casco, E. Zhang, S. Grätz, S. Krause, V. Bon, D. Wallacher, N. Grimm, D. M. Többens, T. Hauß, L. Borchardt, Experimental evidence of confined methane hydrate in hydrophilic and hydrophobic model carbons, J. Phys. Chem. C 123 (2019) 24071-24079.
[60] M. E. Casco, J. S. Albero, A. J. Ramírez-Cuesta, F. Rey, J. L. Jordá, A. Bansode, A. Urakawa, I. Peral, M. M. Escandell, K. Kaneko, F. R. Reinoso, Methane hydrate formation in confined nanospace can surpass nature, Nat. Commun. 6 (2015) 6432.

[61] N. N. Nguyen, A. V. Nguyen, Hydrophobic effect on gas hydrate formation in the presence of additives, Energy Fuels 31 (2017) 10311-10323.
[62] M. S. P. Sansom, P. C. Biggin, Water at the nanoscale, Nature 414 (2001) 157-159.
[63] Z. Li, R.-H. Yoon, Thermodynamics of hydrophobic interaction between silica surfaces coated with octadecyltrichlorosilane, J. Colloid Interface Sci. 392 (2013).
[64] J. Miyawaki, T. Kanda, T. Suzuki, T. Okui, Y. Maeda, K. Kaneko, Macroscopic evidence of enhanced formation of methane nanohydrates in hydrophobic nanospaces, J. Phys. Chem. B 102 (1998) 2187-2192.
[65] N. N. Nguyen, A. V. Nguyen, K. M. Steel, L. X. Dang, M. Galib, Interfacial gas enrichment at hydrophobic surfaces and the origin of promotion of gas hydrate formation by hydrophobic solid particles, J. Phys. Chem. C 121 (2017) 3830-3840.
[66] H. Li, L. Wang, Hydrophobized particles can accelerate nucleation of clathrate hydrates, Fuel 140 (2015) 440-445.
[67] N. N. Nguyen, M. Galib, A. V. Nguyen, Critical Review on Gas Hydrate Formation at Solid Surfaces and in Confined Spaces-Why and How Does Interfacial Regime Matter?, Energy Fuels 34 (2020) 6751-6760.
[68] N. N. Nguyen, A. V. Nguyen, "Nanoreactors" for boosting gas hydrate formation toward energy storage applications, ACS Nano 16 (2022) 11504-11515.
[69] E. J. Beckwee, G. Watson, M. Houlleberghs, D. A. Esteban, S. Bals, P. V. D. Voort, E. Breynaert, J. Martens, G. V. Baron, J. F. M. Denayer, Enabling hydrate-based methane storage under mild operating conditions by periodic mesoporous organosilica nanotubes, Heliyon 9 (2023) e17662.
[70] N. B. Kummamuru, S. W. Verbruggen, S. Lenaerts, P. Perreault, Experimental investigation of methane hydrate formation in the presence of metallic packing, Fuel 323 (2022) 124269.
[71] N. B. Kummamuru, G. Watson, R-G. Ciocarlan, S. W. Verbruggen, P. Cool, P. V. D. Voort, P. Perreault, Accelerated methane storage in clathrate hydrates using mesoporous (Organo-) silica materials, Fuel 354 (2023) 129403.
[72] E. W. Lemmon, M. L. Huber, J. W. Leachman, Revised standardized equation for hydrogen gas densities for fuel consumption applications, J. Res. Natl. Inst. Stand. Technol. 113 (2008) 341-350.
[73] H. P. Veluswamy, P. Linga, Macroscopic kinetics of hydrate formation of mixed hydrates of hydrogen/tetrahydrofuran for hydrogen storage, Int. J. Hydrogen Energy 38 (2013) 4587-4596.
[74] Y. Zhang, G. Bhattacharjee, J. Zheng, P. Linga, Hydrogen storage as clathrate hydrates in the presence of 1,3-dioxolane as a dual-function promoter, J. Chem. Eng. 427 (2022) 131771.
[75] NIST Standard Reference Database, Fundamental physical constants: Avogadro constant, U.S.A.
[76] T. Kawamura, S. Takeya, M. Ohtake, Y. Yamamoto, Enclathration of hydrogen by organic-compound clathrate hydrates, Chem. Eng. Sci. 66 (2011) 2417-2420.
[77] S. Hashimoto, S. Murayama, T. Sugahara, H. Sato, K. Ohgaki, Thermodynamic and Raman spectroscopic studies on H_2+tetrahydrofuran+water and H_2+tetra-n-butyl ammonium bromide+water mixtures containing gas hydrates, Chem. Eng. Sci. 61 (2006) 7884-7888.
[78] R. Ma, H. Zhong, J. Liu, J. Zhong, Y. Yan, J. Zhang, J. Xu, Molecular Insights into Cage Occupancy of Hydrogen Hydrate: A Computational Study, Processes 7 (2019) 699.
[79] H. P. Veluswamy, W. I. Chin, P. Linga, Clathrate hydrates for hydrogen storage: The impact of tetrahydrofuran, tetra-n-butylammonium bromide and cyclopentane as

promoters on the macroscopic kinetics, Int. J. Hydrogen Energy 39 (2014) 16234-16243.
[80] J.-H. Yoon, J. Han, J. Park, S. Choi, S.-H. Yeon, H. Lee, Spectroscopic identification, thermodynamic stability and molecular composition of hydrogen and 1,4-dioxane binary clathrate hydrate, J. Phys. Chem. Solids 69 (2008) 1432-1435.
[81] H. Yoshioka, M. Ota, Y. Sato, M. Watanabe, H. Inomata, R. L. Smith Jr., Decomposition Kinetics and Recycle of BinaryHydrogen-Tetrahydrofuran Clathrate Hydrate, AIChE J. 57 (2011) 265-272.
[82] Y. Nagai, H. Yoshioka, M. Ota, Y. Sato, H. Inomata, R. L. Smith Jr., C. J. Peters, Binary hydrogen-tetrahydrofuran clathrate hydrate formation kinetics and models, AIChE J. 54 (2008) 3007-3016.